ACS Photonics

pubs.acs.org/journal/apchd5

Article

Radiative Thermal Router Based on Tunable Magnetic Weyl Semimetals

Cheng Guo, Bo Zhao, Danhong Huang, and Shanhui Fan*

Cite This: https://dx.doi.org/10.1021/acsphotonics.0c01376

Read Online

ACCESS | Metrics & More | Article Recommendations

ABSTRACT: We theoretically propose and numerically demonstrate a radiative thermal router based on magnetic Weyl semimetals. In designing the thermal router, we utilize two unique properties of optical gyrotropy in magnetic Weyl semimetals: great tunability and nanoscale inhomogeneity. The proposed thermal router consists of three spheres made of magnetic Weyl semimetals, one tunable and two fixed. It can direct a heat flow to a drain of choice by moving the Weyl nodes in the tunable magnetic Weyl semimetal using an external electric, magnetic, or optical field. Such a Weyl-semimetal-based radiative thermal router could enable exciting opportunities in energy harvesting and heat transfer applications.

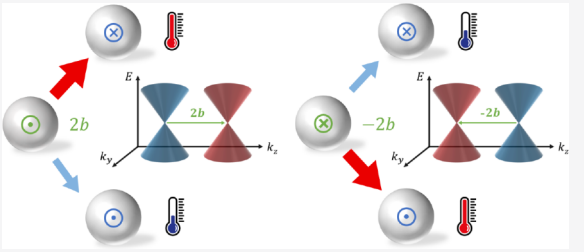

KEYWORDS: *thermal radiation, near-field radiative heat transfer, Weyl semimetal, topological materials*

The exploitation of photon-based heat flow, in both the near-field and far-field regime, is of substantial importance for a wide range of technological applications, including cooling and power generation.[1−6] Motivated by these applications, there are significant efforts in developing schemes for active control of such photon-based heat flow. Notable examples include the development of diodes,[7,8] transistors,[9] switches,[10−12] modulators,[13] and splitters[14] for radiative heat flow.

A key component for active control of photon-based heat flow is a thermal router. The simplest thermal router consists of three terminals: one source and two drains (Figure 1a,b). By turning a control knob to vary the internal status of the thermal router, the heat flux coming from the source can be directed dominantly to either one of the two drains. More complex radiative networks, including multiple channels, can be built by cascading multiple thermal routers. Recently, Song et al. has theoretically proposed to realize thermal routing using an array of graphene-coated SiC nanoparticles.[15] In this scheme, thermal routing is achieved by adjusting the Fermi levels of the graphene layers of individual particles, which is challenging to achieve experimentally.

In this paper, we propose to use tunable magnetic Weyl semimetals as an alternative approach to construct radiative thermal routers. Magnetic Weyl semimetals[16−23] can exhibit extremely large gyrotropic optical responses in the mid-infrared, which originates from their unique topologically nontrivial electronic states and inherent time-reversal symmetry breaking. Moreover, in some magnetic Weyl semimetals, such an optical gyrotropy can be tuned electrically,[24] magnetically,[25,26] and optically.[27] On the basis of such tunable and strong optical gyrotropy, we design a radiative thermal router, as shown in Figure 1c, which consists of three nanoparticles made of Weyl semimetals. We show that efficient thermal routing can be achieved by moving the Weyl nodes in the Brillouin zone of one of the particles using an external electric, magnetic, or optical field.

The rest of this paper is organized as follows: Optical Properties of Magnetic Weyl Semimetals briefly reviews the optical property of magnetic Weyl semimetals relevant to radiative heat transfer. Numerical Results provides the numerical results of the designed radiative thermal router. We conclude in Discussion and Conclusion.

OPTICAL PROPERTIES OF MAGNETIC WEYL SEMIMETALS

In this section, we briefly review the optical properties of magnetic Weyl semimetals that are important for the purpose of radiative thermal routing.

Weyl semimetals are a novel class of three-dimensional gapless topological matter.[16−23] They feature accidental degeneracies in their band structure called Weyl nodes.[28] Each Weyl node acts as a source/drain of Berry curvature in momentum space. The nontrivial topology of the Weyl nodes leads to unique electronic and optical properties. In photonics, Weyl semimetals have been proposed recently for constructing

Received: September 2, 2020

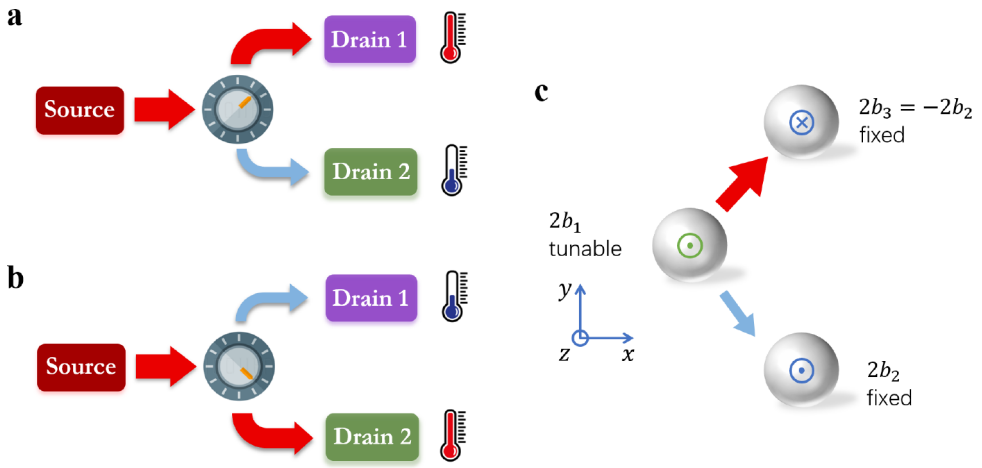

Figure 1. (a, b) Thermal router directs an incoming heat flow to a drain of choice. (c) Radiative thermal router based on tunable Weyl semimetals. The system consists of three spheres of Weyl semimetal nanoparticles: tuning the location of the Weyl node in the momentum space of the center particle results in the thermal routing.

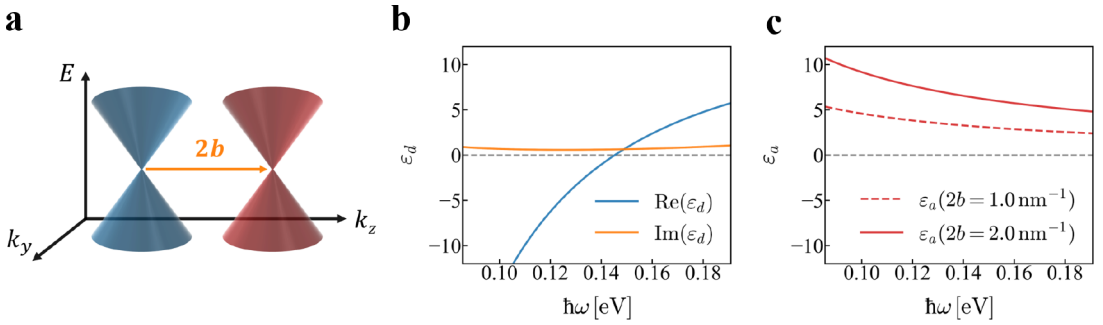

Figure 2. (a) Electronic band structure of a magnetic Weyl semimetal with two Weyl nodes of opposite chirality separated by 2**b** in the wavevector space. (b) The diagonal component ε_d of the permittivity tensor of the Weyl semimetal. (c) The off-diagonal component ε_a of the permittivity tensor of the Weyl semimetal.

compact optical isolators[29] and nonreciprocal thermal emitters.[30−32]

For concreteness, we consider the simplest case of a magnetic Weyl semimetal that hosts two Weyl nodes of opposite chirality at the same energy, with a wavevector separation of 2**b**. Such an ideal Weyl semimetal phase has been experimentally realized recently in materials such as $EuCd_2As_2$.[33]

If we choose the crystal orientation of the Weyl semimetal such that **b** is along the $\hat{z}$ direction, $\mathbf{b} = b\hat{z}$, the effective permittivity tensor becomes

$$\overline{\overline{\varepsilon}} = \begin{pmatrix} \varepsilon_d & i\varepsilon_a & 0 \\ -i\varepsilon_a & \varepsilon_d & 0 \\ 0 & 0 & \varepsilon_d \end{pmatrix} \tag{1}$$

where $\varepsilon_a = be^2/(2\pi^2\hbar\omega)$. Thus, $\overline{\overline{\varepsilon}}$ is asymmetric and breaks Lorentz reciprocity. The diagonal term ε_d is calculated by using the Kubo-Greenwood formalism within the random phase approximation to a two-band model with spin degeneracy:[34−36]

$$\varepsilon_d = \varepsilon_b + \frac{ir_s g}{6\Omega_0}\Omega G(\Omega/2) - \frac{r_s g}{6\pi\Omega_0}\left\{\frac{4}{\Omega}\left[1 + \frac{\pi^2}{3}\left(\frac{k_B T}{E_F(T)}\right)^2\right] + 8\Omega\int_0^{\xi_c}\frac{G(\xi) - G(\Omega/2)}{\Omega^2 - 4\xi^2}\xi d\xi\right\} \tag{2}$$

Here, ε_b is the background permittivity, E_F is the chemical potential, $\Omega_0 = \hbar\omega/E_F$ is the normalized real frequency, $\Omega = \hbar(\omega + i\tau^{-1})/E_F$ is the normalized complex frequency, τ^{-1} is the Drude damping rate, $G(E) = n(-E) - n(E)$, with $n(E)$ as the Fermi distribution function, $r_s = e^2/4\pi\epsilon_0\hbar v_F$ is the effective fine-structure constant, v_F is the Fermi velocity, g is the number of Weyl points, and $\xi_c = E_c/E_F$, with E_c as the cutoff energy beyond which the band dispersion is no longer linear.[35] Following ref 36, in this work we use the parameters $\varepsilon_b = 6.2$, $\xi_c = 3$, $\tau = 450$ fs, $g = 2$, $b = 8.5 \times 10^8$ m^{-1}, $v_F = 0.83 \times 10^5$ m/s, and $E_F = 0.15$ eV at $T = 300$ K.

We plot the calculated frequency dispersion of ε_d and ε_a in Figure 2b and c, respectively. In the frequency range of interest, the diagonal component ε_d can be well described by a usual lossy Drude model (Figure 2b). The off-diagonal component ε_a strongly depends on the Weyl node separation 2***b*** (Figure 2c). The magnitude of ε_a can be comparable to that of ε_d in the mid-infrared wavelengths, which indicates a highly unusual and extremely large gyrotropic response. In comparison, in commonly used gyrotropic medium at the mid-infrared wavelength range, such as heavily doped semiconductor under

https://dx.doi.org/10.1021/acsphotonics.0c01376
ACS Photonics XXXX, XXX, XXX−XXX

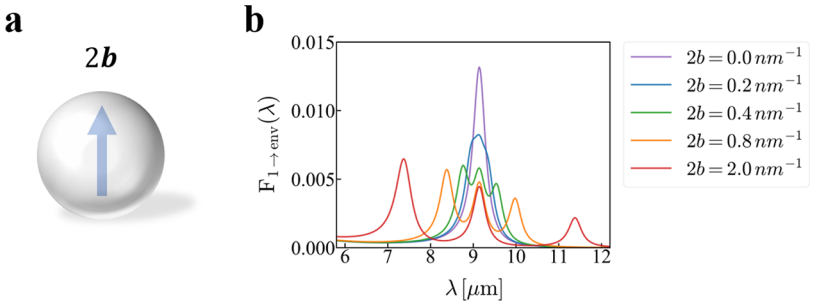

Figure 3. (a) Thermal radiation from a nanosphere made of magnetic Weyl semimetal. The sphere has a radius of 100 nm. The material parameters are given in the main text. The Weyl node separation is $2\boldsymbol{b}$. (b) The spectra of transmission coefficient from the nanosphere to the environment at different values of $2b$.

external magnetic field, $|\epsilon_a|/|\epsilon_d| \sim 10^{-3}$, even under a strong magnetic field of a few Tesla.[37] Such a strong gyrotropy originates from the unique topologically nontrivial electronic states and inherent time reversal symmetry breaking in magnetic Weyl semimetals and has been utilized to construct compact isolator[29] and nonreciprocal thermal emitters without the need for an external magnetic field.[30,31]

As shown above, the optical gyrotropy of Weyl semimetals is determined by their band topology, especially the locations of Weyl nodes in the Brillouin zone. Therefore, the gyrotropic response can be tuned by moving the Weyl points around in the Brillouin zone. In most Weyl semimetals, the position of the Weyl points in the Brillouin zone is fixed. (Here we refer to these materials as "fixed" Weyl semimetals.) Recently, it was discovered that there exist Weyl semimetals whose Weyl nodes can be moved easily under moderate external fields. Such materials are referred to as "tunable" Weyl semimetals. The manipulation of Weyl nodes has been achieved electrically,[24] magnetically,[25,26] and optically.[27] In particular, magnetic textures in magnetic Weyl semimetals can provide convenient handles for manipulating the Weyl nodes with a high modulation speed by applying either an external magnetic field[25,26] or an electric current.[24] For example, it has been shown experimentally[26] that, in Co_2MnAl, an external magnetic field $B \approx \pm 1$ T can induce a giant Weyl node separation $2b \approx \pm 11$ nm^{-1}.

In addition to the great tunability of optical gyrotropy, there is another unique opportunity offered by magnetic Weyl semimetals: nanoscale inhomogeneity of optical gyrotropy. Consider clusters of nanoparticles made of magnetic Weyl semimetals. Since the optical gyrotropy of each particle is determined by the band structure associated with each crystal, particles with different crystal orientations can have very different gyrotropic response. This is in sharp contrast with clusters of magneto-optical particles, the optical gyrotropy of which is solely determined by the external magnetic field.[37,38] And, hence, it is hard to achieve nanoscale inhomogeneity of optical gyrotropy in such systems.

NUMERICAL RESULTS

In this section, we numerically demonstrate a radiative thermal router based on the optical properties of both fixed and tunable Weyl semimetals.

We consider clusters of N spherical nanoparticles made of magnetic Weyl semimetals that exchange heat via radiation with each other and an environment (denoted as env). We label the environment and the bodies as $\{0 \equiv \text{env}, 1, 2, ..., N\}$. For concreteness, we assume the material parameters of all the Weyl semimetal particles take the values as described in Optical Properties of Magnetic Weyl Semimetals, except that the Weyl node separation $2\boldsymbol{b}_i$ ($i = 1, 2, ..., N$) may be different for different particles. All the nanospheres are assumed to have the same radius of 100 nm.

For radiative heat transfer, one considers the spectral heat flux to body j due to thermal noise sources in body i of temperature T_i:

$$S_{i\to j}(\omega) = \frac{\Theta(\omega, T_i)}{2\pi} F_{i\to j}(\omega) \tag{3}$$

where $\Theta(\omega, T_i) = \hbar\omega/[\exp(\hbar\omega/k_B T_i) - 1]$, and $F_{i\to j}(\omega)$ denotes the temperature-independent transmission coefficient from body i to j.[39] The integrated heat flux from body i to j is

$$S_{i\to j} \equiv \int_0^\infty d\omega S_{i\to j}(\omega) = \int_0^\infty d\omega \frac{\Theta(\omega, T_i)}{2\pi} F_{i\to j}(\omega) \tag{4}$$

In the linear response regime where the systems are near the thermal equilibrium (i.e., $T_i = T_{eq} + \Delta T_i$, $T_{env} = T_{eq}$, with $\Delta T_i \ll T_{eq}$), the integrated heat flux from body i to body j is

$$S_{i\to j} = S_{i\to j}^{(eq)} + G_{i\to j}\Delta T_i \tag{5}$$

where

$$S_{i\to j}^{(eq)} = \int_0^\infty d\omega \frac{\Theta(\omega, T_{eq})}{2\pi} F_{i\to j}(\omega) \tag{6}$$

is the integrated heat flux from body i to body j at equilibrium, and

$$G_{i\to j} \equiv \int_0^\infty \frac{d\omega}{2\pi} \frac{\partial\Theta(\omega, T)}{\partial T}\Big|_{T=T_{eq}} F_{i\to j}(\omega) \tag{7}$$

is the thermal conductance from body i to body j at T_{eq}. In this work, we calculate the transmission coefficients following the framework developed in ref 39, which uses a self-consistent scattered field approach within the framework of fluctuational electrodynamics and is, in principle, exact.

To elucidate the physics, we first consider thermal emission from one nanosphere ($N = 1$) made of a magnetic Weyl semimetal with tunable Weyl node separation $2\boldsymbol{b}$ (Figure 3a). We plot the transmission coefficient spectra from the sphere to the environment in Figure 3b. When $2b = 0$, the emission spectrum exhibits a single peak at the wavelength $\lambda = 9.1$ μm, which corresponds to the localized plasmon mode. This mode is dipole-like and is 3-fold degenerate by symmetry. When $2b \neq 0$, such a 3-fold degenerate mode splits into three singly degenerate modes, which manifest as three peaks in the emission spectrum when $2b$ is large. The splitting of the

https://dx.doi.org/10.1021/acsphotonics.0c01376
ACS Photonics XXXX, XXX, XXX−XXX

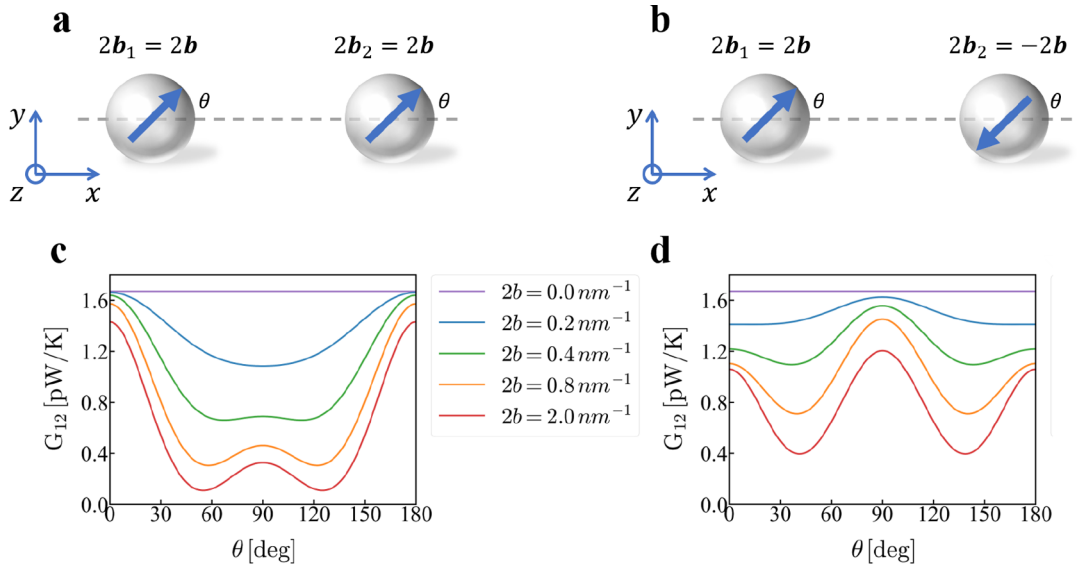

Figure 4. Radiative heat transfer between two nanospheres made of magnetic Weyl semimetals. The material parameters are given in the main text. Both spheres have the same radius of 100 nm. The centers of the two spheres are separated by 320 nm along the x-axis. (a) The parallel configuration where the Weyl node separation $2\boldsymbol{b}_1 = 2\boldsymbol{b}_2$. b denotes the magnitude of $\boldsymbol{b}_1$ and $\boldsymbol{b}_2$, and θ denotes the angle between $\boldsymbol{b}_1$ (and $\boldsymbol{b}_2$) and the x-axis. (b) The antiparallel configuration where the Weyl node separation $2\boldsymbol{b}_1 = -2\boldsymbol{b}_2$. b denotes the magnitude of $\boldsymbol{b}_1$ and $\boldsymbol{b}_2$, and θ denotes the angle between $\boldsymbol{b}_1$ (and $-\boldsymbol{b}_2$) and the x-axis. (c) The thermal conductance $G_{1\to2} = G_{2\to1} \equiv G_{12}$ as functions of θ and b for the parallel configuration as shown in (a). (d) The thermal conductance $G_{1\to2} = G_{2\to1} \equiv G_{12}$ as functions of θ and b for the antiparallel configuration, as shown in (b).

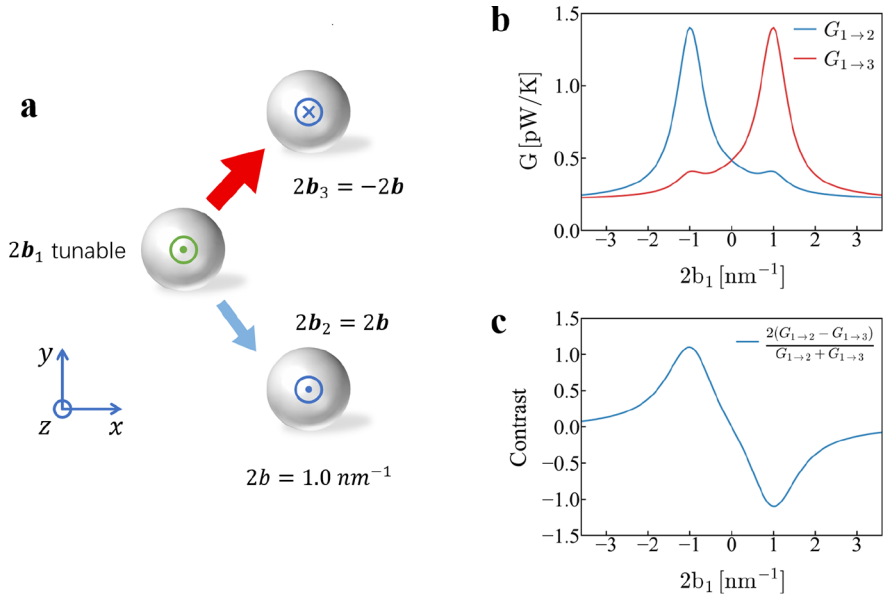

Figure 5. (a) Radiative thermal router consisting of three spheres made of magnetic Weyl semimetals. All the three spheres have the same radius of 100 nm. The centers of the three spheres form an isosceles triangle in the x−y plane with a leg length of 320 nm, a base length of 554 nm, and a vertex angle of 120°. The sphere 1 located at the apex is made of a tunable magnetic Weyl semimetal with the Weyl node separation $2\boldsymbol{b}_1$ along the z-direction controlled by an external field. Spheres 2 and 3 are made of fixed magnetic Weyl semimetals with $2\boldsymbol{b}_2 = 1.0\ \mathrm{nm}^{-1}$ and $2\boldsymbol{b}_3 = -1.0\ \mathrm{nm}^{-1}$ along the z-direction, respectively. (b) Thermal conductance $G_{1\to2}$ and $G_{1\to3}$ as a function of $2b_1$. (c) The contrast $2(G_{1\to2} - G_{1\to3})/(G_{1\to2} + G_{1\to3})$ as a function of $2b_1$.

resonant frequencies increases as $2b$ increases. One of the three modes is b-independent, while the other two are strongly b-dependent.[40] These two b-dependent modes are the "circular" modes where the modal fields rotate clockwise and counterclockwise around the $\boldsymbol{b}$ direction, respectively.[41] Such a rotation is induced by the gyrotropic response. The b-independent mode is the "non-rotating" mode that exhibits zero angular momentum.

Then we consider two spheres made of magnetic Weyl semimetals ($N = 2$). We study two different configurations, as shown in Figure 4a,b. In both cases, the centers of the two spheres are separated by 320 nm along the x-axis. The two cases differ in the configuration of Weyl node separations. In the first case called the parallel configuration (Figure 4a), the Weyl node separations of the two spheres are the same in magnitude and parallel in direction, that is, $2\boldsymbol{b}_1 = 2\boldsymbol{b}_2$. In the second case, called the antiparallel configuration (Figure 4b),

https://dx.doi.org/10.1021/acsphotonics.0c01376
ACS Photonics XXXX, XXX, XXX−XXX

the Weyl node separations of the two spheres are the same in magnitude and antiparallel in direction, that is, $2\boldsymbol{b}_1 = -2\boldsymbol{b}_2$. In both cases, we denote the magnitude of $\boldsymbol{b}_1$ and $\boldsymbol{b}_2$ as b, and the angle between $\boldsymbol{b}_1$ and the x-axis as θ. Accordingly, the angle between $\boldsymbol{b}_2$ and the x-axis is θ in the parallel configuration and $\pi + \theta$ in the antiparallel configuration.

We numerically calculate the thermal conductance $G_{1\to2}$ and $G_{2\to1}$ as functions of θ and b. Figure 4c and d show the results for the parallel and antiparallel configurations, respectively. We verify that $G_{1\to2} = G_{2\to1} \equiv G_{12}$ for all θ and b in both configurations, as required by the inversion symmetry in the parallel configuration and the 2-fold rotation symmetry around the z-axis in the antiparallel configuration, respectively.[42] (Here, we note that $2\boldsymbol{b}$ is an axial vector.) For each given value of θ, G_{12} monotonically decreases as b increases in both configurations. This results from the strong spectral splitting and shift of the localized plasmon modes induced by the gyrotropic responses, as shown in Figure 3b. Such an effect is similar to the giant thermal magnetoresistance between two magneto-optical plasmonic particles.[40] For a given value of b, G_{12} has a θ dependence in each configuration. This angular dependence arises from the anisotropic thermal emission of these particles induced by the optical gyrotropy, which leads to the corresponding anisotropy in the photon tunneling. Importantly, such a θ dependence is significantly different for the parallel and antiparallel configurations. The contrast is especially sharp when $\theta = 90°$: at the same value of b, G_{12} in the antiparallel configuration is much larger than that in the parallel configuration. This can be intuitively understood from the condition of mode matching. When $\theta = 90°$, in the parallel (antiparallel) configuration the "circular" modes in the two spheres that are frequency matched have the same (opposite) sense of rotation around the y-axis. The photon tunneling is more efficient when the modes with the opposite sense of rotation are frequency matched, since in this case at the gap region between the particles, the fields of the modes in the two particles move in the same direction and, hence, are approximately phase-matched. Therefore, G_{12} becomes larger in the antiparallel configuration when $\theta = 90°$.

Based on the above observations, we provide a concrete design of radiative thermal router using three spheres made of magnetic Weyl semimetals, as shown in Figure 5a. The centers of the three spheres form an isosceles triangle in the x−y plane with a leg length of 320 nm, a base length of 554 nm, and a vertex angle of 120°. The sphere 1 located at the apex is made of a tunable magnetic Weyl semimetal with the Weyl node separation $2\boldsymbol{b}_1$ along the z-direction. $2\boldsymbol{b}_1$ is controlled by an external field, which provides the control knob of the radiative thermal router (cf. Figure 1). The other spheres 2 and 3 are made of fixed magnetic Weyl semimetals with $2\boldsymbol{b}_2 = 1.0\ \mathrm{nm}^{-1}$ and $2\boldsymbol{b}_3 = -1.0\ \mathrm{nm}^{-1}$ along the z-direction, respectively.

We calculate and plot in Figure 5b the thermal conductance $G_{1\to2}$ and $G_{1\to3}$ as a function of b_1. There is a relation $G_{1\to2}(b_1) = G_{1\to2}(-b_1)$, as required by symmetry. Importantly, $G_{1\to2}$ and $G_{1\to3}$ strongly depend on $2\boldsymbol{b}_1$. $G_{1\to2}$ exhibits a sharp peak when $2\boldsymbol{b}_1 = -2\boldsymbol{b}_2 = -1.0\ \mathrm{nm}^{-1}$. This can also be explained by mode matching: when $2\boldsymbol{b}_1 = -2\boldsymbol{b}_2$, the modes with the opposite sense of rotation in spheres 1 and 2 are frequency matched, and photon tunneling is more efficient. Similarly, $G_{1\to3}$ exhibits a sharp peak when $2\boldsymbol{b}_1 = -2\boldsymbol{b}_3 = 1.0\ \mathrm{nm}^{-1}$. As a side note, the numerical results indicate that, even though such a system is nonreciprocal, the nonreciprocal effect is weak in radiative heat transfer: $G_{1\to2} \approx G_{2\to1}$ and $G_{1\to3} \approx G_{3\to1}$.

Since $G_{1\to2}$ and $G_{1\to3}$ exhibit very different behaviors when $2\boldsymbol{b}_1$ is varied, the structure can achieve the required functionality of radiative thermal routing. To evaluate the performance quantitatively, we plot the contrast function, defined as $2(G_{1\to2} - G_{1\to3})/(G_{1\to2} + G_{1\to3})$, as a function of b_1 in Figure 5c. Since the thermal conductance is always nonnegative, the contrast is bounded below by −2 and above by 2 by definition. In our structure, the contrast reaches the maximum value 1.1 when $2\boldsymbol{b}_1 = -1.0\ \mathrm{nm}^{-1}$ and the negative maximum value −1.1 when $2\boldsymbol{b}_1 = 1.0\ \mathrm{nm}^{-1}$, which indicates a good performance of radiative thermal routing. Moreover, we have numerically verified that the contrast function plotted in Figure 5c is not sensitive to modest variations of the sphere radii or the side lengths of the isosceles triangle if the vertex angle is fixed. This indicates the robustness of the radiative thermal routering.

DISCUSSION AND CONCLUSION

In this work, we focus on the frequency and wavevector regime where the nonreciprocal surface plasmon modes are associated with the collective behavior of bulk carriers close to the surface. Weyl semimetals also feature topological Fermi arc surface states,[43,44] which can support surface plasmon modes.[45] The study of nonreciprocal thermal emission from such Fermi arc plasmons will be presented in the future.

In conclusion, we have demonstrated a radiative thermal router based on magnetic Weyl semimetals. The design utilizes two unique properties of optical gyrotropy in magnetic Weyl semimetals: great tunability and nanoscale inhomogeneity. Such a thermal router consists of three spheres made of magnetic Weyl semimetals: one tunable and two fixed. It can direct a heat flow to a drain of choice by moving the Weyl nodes in the tunable magnetic Weyl semimetal with an external electric, magnetic, or optical field. The designed Weyl-semimetal-based radiative thermal router could enable exciting opportunities in energy harvesting and heat transfer applications, in an analogy with controlling electrical current in integrated circuits or light propagation in photonic circuits.

AUTHOR INFORMATION

Corresponding Author

Shanhui Fan − *Ginzton Laboratory and Department of Electrical Engineering, Stanford University, Stanford, California 94305, United States;* orcid.org/0000-0002-0081-9732; Email: shanhui@stanford.edu

Authors

Cheng Guo − *Department of Applied Physics, Stanford University, Stanford, California 94305, United States;* orcid.org/0000-0003-4913-8150

Bo Zhao − *Ginzton Laboratory and Department of Electrical Engineering, Stanford University, Stanford, California 94305, United States;* orcid.org/0000-0002-3648-6183

Danhong Huang − *Air Force Research Laboratory, Space Vehicles Directorate, Kirtland Air Force Base, Albuquerque, New Mexico 87117, United States*

Complete contact information is available at: https://pubs.acs.org/10.1021/acsphotonics.0c01376

Notes

The authors declare no competing financial interest.

https://dx.doi.org/10.1021/acsphotonics.0c01376
ACS Photonics XXXX, XXX, XXX−XXX

■ ACKNOWLEDGMENTS

C.G. thanks Dr. Yu Guo and Dr. Linxiao Zhu for helpful discussion. This work is supported by an Army Research Office (ARO) MURI Program (Grant No. W911NF-19-1-0279) and by the Defense Advanced Research Project Agency (DARPA; Grant No. HR00111820046). D.H. thanks the support from the Air Force Office of Scientific Research (AFOSR). D.H is also supported by the DoD Laboratory-University Collaborative Initiative (LUCI) program.

■ REFERENCES

(1) Planck, M. *The Theory of Heat Radiation*; Dover Publications: New York, 1991.
(2) Rytov, S. M.; Kravtsov, Y. A.; Tatarskii, V. I. *Principles of Statistical Radiophysics 3: Elements of Random Fields*; Springer-Verlag: Berlin, Heidelberg, 1989.
(3) Chen, G. *Nanoscale Energy Transport and Conversion: A Parallel Treatment of Electrons, Molecules, Phonons, and Photons*; Oxford University Press: Oxford, 2005.
(4) Zhang, Z. M. *Nano/Microscale Heat Transfer*; McGraw-Hill: New York, 2007.
(5) Howell, J. R.; Mengüç, M. P.; Siegel, R. *Thermal Radiation Heat Transfer*, 6th ed.; CRC Press: London, 2016.
(6) Fan, S. Thermal Photonics and Energy Applications. *Joule* **2017**, *1*, 264−273.
(7) Otey, C. R.; Lau, W. T.; Fan, S. Thermal Rectification through Vacuum. *Phys. Rev. Lett.* **2010**, *104*, 154301.
(8) Ben-Abdallah, P.; Biehs, S.-A. Phase-Change Radiative Thermal Diode. *Appl. Phys. Lett.* **2013**, *103*, 191907.
(9) Ben-Abdallah, P.; Biehs, S.-A. Near-Field Thermal Transistor. *Phys. Rev. Lett.* **2014**, *112*, No. 044301.
(10) Yang, Y.; Basu, S.; Wang, L. Vacuum Thermal Switch Made of Phase Transition Materials Considering Thin Film and Substrate Effects. *J. Quant. Spectrosc. Radiat. Transfer* **2015**, *158*, 69−77.
(11) Gu, W.; Tang, G.-H.; Tao, W.-Q. Thermal Switch and Thermal Rectification Enabled by Near-Field Radiative Heat Transfer between Three Slabs. *Int. J. Heat Mass Transfer* **2015**, *82*, 429−434.
(12) Ilic, O.; Thomas, N. H.; Christensen, T.; Sherrott, M. C.; Soljačić, M.; Minnich, A. J.; Miller, O. D.; Atwater, H. A. Active Radiative Thermal Switching with Graphene Plasmon Resonators. *ACS Nano* **2018**, *12*, 2474−2481.
(13) Biehs, S.-A.; Rosa, F. S. S.; Ben-Abdallah, P. Modulation of Near-Field Heat Transfer between Two Gratings. *Appl. Phys. Lett.* **2011**, *98*, 243102.
(14) Ben-Abdallah, P.; Belarouci, A.; Frechette, L.; Biehs, S.-A. Heat Flux Splitter for Near-Field Thermal Radiation. *Appl. Phys. Lett.* **2015**, *107*, No. 053109.
(15) Song, J.; Lu, L.; Li, B.; Zhang, B.; Hu, R.; Zhou, X.; Cheng, Q. Thermal Routing via Near-Field Radiative Heat Transfer. *Int. J. Heat Mass Transfer* **2020**, *150*, 119346.
(16) Xu, S.-Y.; et al. Discovery of a Weyl Fermion Semimetal and Topological Fermi Arcs. *Science* **2015**, *349*, 613−617.
(17) Lv, B. Q.; Weng, H. M.; Fu, B. B.; Wang, X. P.; Miao, H.; Ma, J.; Richard, P.; Huang, X. C.; Zhao, L. X.; Chen, G. F.; Fang, Z.; Dai, X.; Qian, T.; Ding, H. Experimental Discovery of Weyl Semimetal TaAs. *Phys. Rev. X* **2015**, *5*, No. 031013.
(18) Xu, S.-Y.; et al. Experimental Discovery of a Topological Weyl Semimetal State in TaP. *Science Advances* **2015**, *1*, No. e1501092.
(19) Belopolski, I.; et al. Discovery of Topological Weyl Fermion Lines and Drumhead Surface States in a Room Temperature Magnet. *Science* **2019**, *365*, 1278−1281.
(20) Morali, N.; Batabyal, R.; Nag, P. K.; Liu, E.; Xu, Q.; Sun, Y.; Yan, B.; Felser, C.; Avraham, N.; Beidenkopf, H. Fermi-Arc Diversity on Surface Terminations of the Magnetic Weyl Semimetal $Co_3Sn_2S_2$. *Science* **2019**, *365*, 1286−1291.
(21) Liu, D. F.; et al. Magnetic Weyl Semimetal Phase in a Kagomé Crystal. *Science* **2019**, *365*, 1282−1285.
(22) Kuroda, K.; et al. Evidence for Magnetic Weyl Fermions in a Correlated Metal. *Nat. Mater.* **2017**, *16*, 1090−1095.
(23) Hirschberger, M.; Kushwaha, S.; Wang, Z.; Gibson, Q.; Liang, S.; Belvin, C. A.; Bernevig, B. A.; Cava, R. J.; Ong, N. P. The Chiral Anomaly and Thermopower of Weyl Fermions in the Half-Heusler GdPtBi. *Nat. Mater.* **2016**, *15*, 1161−1165.
(24) Tsai, H.; Higo, T.; Kondou, K.; Nomoto, T.; Sakai, A.; Kobayashi, A.; Nakano, T.; Yakushiji, K.; Arita, R.; Miwa, S.; Otani, Y.; Nakatsuji, S. Electrical Manipulation of a Topological Antiferromagnetic State. *Nature* **2020**, *580*, 608−613.
(25) Ray, R.; Sadhukhan, B.; Richter, M.; Facio, J. I.; van den Brink, J. Tunable Chirality of Noncentrosymmetric Magnetic Weyl Semimetals. *arXiv:2006.10602 [cond-mat]* **2020**, na.
(26) Li, P.; Koo, J.; Ning, W.; Li, J.; Miao, L.; Min, L.; Zhu, Y.; Wang, Y.; Alem, N.; Liu, C.-X.; Mao, Z.; Yan, B. Giant Room Temperature Anomalous Hall Effect and Tunable Topology in a Ferromagnetic Topological Semimetal Co_2MnAl. *Nat. Commun.* **2020**, *11*, 3476.
(27) Sie, E. J.; et al. An Ultrafast Symmetry Switch in a Weyl Semimetal. *Nature* **2019**, *565*, 61−66.
(28) Armitage, N. P.; Mele, E. J.; Vishwanath, A. Weyl and Dirac Semimetals in Three-Dimensional Solids. *Rev. Mod. Phys.* **2018**, *90*, No. 015001.
(29) Asadchy, V. S.; Guo, C.; Zhao, B.; Fan, S. Sub-Wavelength Passive Optical Isolators Using Photonic Structures Based on Weyl Semimetals. *Adv. Opt. Mater.* **2020**, *8*, 2000100.
(30) Zhao, B.; Guo, C.; Garcia, C. A. C.; Narang, P.; Fan, S. Axion-Field-Enabled Nonreciprocal Thermal Radiation in Weyl Semimetals. *Nano Lett.* **2020**, *20*, 1923−1927.
(31) Tsurimaki, Y.; Qian, X.; Pajovic, S.; Han, F.; Li, M.; Chen, G. Large Nonreciprocal Absorption and Emission of Radiation in Type-I Weyl Semimetals with Time Reversal Symmetry Breaking. *Phys. Rev. B: Condens. Matter Mater. Phys.* **2020**, *101*, 165426.
(32) Ott, A.; Biehs, S.-A.; Ben-Abdallah, P. Anomalous Photon Thermal Hall Effect. *Phys. Rev. B: Condens. Matter Mater. Phys.* **2020**, *101*, 241411.
(33) Soh, J.-R.; et al. Ideal Weyl Semimetal Induced by Magnetic Exchange. *Phys. Rev. B: Condens. Matter Mater. Phys.* **2019**, *100*, 201102.
(34) Hofmann, J.; Das Sarma, S. Surface Plasmon Polaritons in Topological Weyl Semimetals. *Phys. Rev. B: Condens. Matter Mater. Phys.* **2016**, *93*, 241402.
(35) Kotov, O. V.; Lozovik, Y. E. Dielectric Response and Novel Electromagnetic Modes in Three-Dimensional Dirac Semimetal Films. *Phys. Rev. B: Condens. Matter Mater. Phys.* **2016**, *93*, 235417.
(36) Kotov, O. V.; Lozovik, Y. E. Giant Tunable Nonreciprocity of Light in Weyl Semimetals. *Phys. Rev. B: Condens. Matter Mater. Phys.* **2018**, *98*, 195446.
(37) Zhu, L.; Fan, S. Near-Complete Violation of Detailed Balance in Thermal Radiation. *Phys. Rev. B: Condens. Matter Mater. Phys.* **2014**, *90*, 220301.
(38) Guo, C.; Guo, Y.; Fan, S. Relation between Photon Thermal Hall Effect and Persistent Heat Current in Nonreciprocal Radiative Heat Transfer. *Phys. Rev. B: Condens. Matter Mater. Phys.* **2019**, *100*, 205416.
(39) Zhu, L.; Guo, Y.; Fan, S. Theory of Many-Body Radiative Heat Transfer without the Constraint of Reciprocity. *Phys. Rev. B: Condens. Matter Mater. Phys.* **2018**, *97*, No. 094302.
(40) Latella, I.; Ben-Abdallah, P. Giant Thermal Magnetoresistance in Plasmonic Structures. *Phys. Rev. Lett.* **2017**, *118*, 173902.
(41) Abraham Ekeroth, R. M.; Ben-Abdallah, P.; Cuevas, J. C.; García-Martín, A. Anisotropic Thermal Magnetoresistance for an Active Control of Radiative Heat Transfer. *ACS Photonics* **2018**, *5*, 705−710.
(42) Guo, C.; Fan, S. Theoretical Constraints on Reciprocal and Non-Reciprocal Many-Body Radiative Heat Transfer. *Phys. Rev. B: Condens. Matter Mater. Phys.* **2020**, *102*, No. 085401.

https://dx.doi.org/10.1021/acsphotonics.0c01376
ACS Photonics XXXX, XXX, XXX−XXX

(43) Zheng, H.; et al. Atomic-Scale Visualization of Quantum Interference on a Weyl Semimetal Surface by Scanning Tunneling Microscopy. *ACS Nano* **2016**, *10*, 1378−1385.
(44) Belopolski, I.; et al. Criteria for Directly Detecting Topological Fermi Arcs in Weyl Semimetals. *Phys. Rev. Lett.* **2016**, *116*, No. 066802.
(45) Song, J. C. W.; Rudner, M. S. Fermi Arc Plasmons in Weyl Semimetals. *Phys. Rev. B: Condens. Matter Mater. Phys.* **2017**, *96*, 205443.

https://dx.doi.org/10.1021/acsphotonics.0c01376
ACS Photonics XXXX, XXX, XXX−XXX